

Wave-shape profiles in a coupled inductor-capacitor network with nonlinear dispersionGuy Roger Deffo,^{1,*} Serge Bruno Yamgoué,^{2,†} and François Beceau Pelap^{1,‡}¹*Unité de Recherche de Mécanique et de Modélisation des Systèmes Physiques, Département de Physique, Université de Dschang, BP 69 Dschang, Cameroon*²*Department of Physics, Higher Teachers Training College Bambili, University of Bamenda, P.O. Box 39, Bamenda, Cameroon*

(Received 20 April 2019; published 19 August 2019)

In this work, the qualitative structures of traveling waves are investigated in a bidimensional inductor-capacitor network with quadratic nonlinear dispersion. Applying the continuum limit approximation, we show that the dynamics of small-amplitude signals in the network can be governed by a $(2 + 1)$ -dimensional partial differential equation. Using a simple transformation, we reduce the given equation to a nonlinear ordinary differential equation. By means of the phase plane analysis and depending on the wave velocity of the signals that are to propagate in the lattice, we present all phase portraits of the dynamical system. Parametric representations for solitary-wave solutions corresponding to the various phase portrait trajectories under different parameter conditions are derived. The results of our study demonstrate that the nonlinear dispersion in the network leads to a number of interesting solitary-wave profiles, e.g., bright-dark solitons and gray-gray solitons, which have not been observed for the same model when the dispersion is assumed linear. The two-dimensional graphics of all the solutions obtained in this paper are given.

DOI: [10.1103/PhysRevE.100.022214](https://doi.org/10.1103/PhysRevE.100.022214)**I. INTRODUCTION**

Nonlinear transmission lines (NLTLs) are now well established as potential models for the study of the behavior of nonlinear excitations inside dispersive media. This is due to both their applications in signal processing in the microwave range and their capability to support solitons, which are localized disturbances which act somewhat as particles [1]. Consequently, many theoretical and experimental studies have been envisaged to analyze the dynamics of different models of NLTLs. Comte and Marquié used a model of NLTLs to experiment on the propagation of compactonlike kinks in a diffusion-reaction chain [2]. Pelap *et al.* studied the dynamics and properties of modulated waves in a modified Noguchi electrical transmission line [3]. The same model with nearest-neighbor interactions has been used to show that two bright solitary signals or a bright and a dark solitary signal may simultaneously propagate at the same frequency through the network [4]. Recently, Deffo *et al.* studied the dynamics of a nonlinear two-dimensional discrete electrical lattice [5]. They showed that the dynamics of the small-amplitude signals in the network can be governed by a $(2 + 1)$ -dimensional generalized modified Zakharov-Kuznetsov equation. Several other models of NLTLs have also been examined in the literature [6,7].

Despite this great interest in NLTLs and their wide range of applications, we note that very few investigations have been done on the dynamics of nonlinear excitations in the NLTLs with nonlinear dispersion [8–10]. Nevertheless, in real

physical systems, nonlinear dispersion can be introduced in order to improve the understanding of some physics phenomena such as the dispersion of particles in suspension, the migration of magma, the formation of liquid drops, and the thermodynamic properties of anharmonic lattices [8].

In this respect, we set out in the present paper to undertake the investigation of a two-dimensional NLTL that includes nonlinear dispersion. We are interested in particular in the single and two solitary-wave solutions for this NLTL. The paper is organized as follows. Section II presents a brief description of our model and its dynamics equation. In Sec. III we discuss the bifurcations of phase portraits of the dynamical system as a function of the wave velocity v_0 . In Sec. IV we determine the parametric representations for solitary wave solutions of the characteristic network equation. We also present here the two-dimensional graphical profiles of these solutions. In Sec. V we summarize and state the main conclusion of this paper.

II. MODEL DESCRIPTION AND DYNAMIC EQUATION

We consider a nonlinear network in which there are many identical lines transversely or longitudinally coupled to one another by an inductor L_2 or L_1 and a capacitor C_2 or C_1 mounted in parallel, as shown in Fig. 1. The nodes in the system are labeled with two discrete coordinates n and m , where n specifies the nodes in the direction of propagation of the pulse and m labels the lines in the transverse direction. The standard nonlinearity is introduced in the network by a varicap diode with differential capacitance $C(V_b + V_{n,m}) = dQ_{n,m}/dV_{n,m}$, which is a nonlinear function of the voltage $V_{n,m}$. For low voltages around the dc bias voltage V_b , the dependence of $Q_{n,m}(V_{n,m})$ at the (n, m) th node can be approximated by [11] $Q_{n,m} = C_0(V_{n,m} - \alpha V_{n,m}^2)$, where C_0 is

*guyrdeffo@yahoo.fr

†sergebruno@yahoo.fr

‡fbpelap@yahoo.fr, francois.pelap@univ-dschang.org

a characteristic capacitance and α is a positive nonlinear parameter of the electrical stored charge. The capacitance-voltage relationship in the series branch is Taylor expanded to first order as [1,12] $C_i(V_{n,m}) = C_{0i}(1 - 2\delta_i V_{n,m})$ with $i = 1, 2$. For $\delta_i = 0$, C_i leads to a linear dispersion parameter $C_i(V_{n,m}) = C_{0i}$; henceforth, C_{0i} will be called the linear dispersion parameter of the network. Assuming that such capacitors can actually exist, we can discuss the fundamental characterization of the network of Fig. 1 and investigate

the dynamics of its traveling waves. We apply Kirchhoff laws to the circuit loop of Fig. 1 and obtain the circuit equation as $L_1 \frac{dI_{n,m}^1}{dt} = V_{n,m} - V_{n+1,m}$, $L_2 \frac{dI_{n,m}^2}{dt} = V_{n,m} - V_{n,m+1}$, $I_{n,m}^1 - I_{n,m}^{1,1} = C_{01} \frac{d}{dt} [(V_{n-1,m} - V_{n,m}) - \delta_1 (V_{n-1,m} - V_{n,m})^2]$, $I_{n,m}^2 - I_{n,m}^{2,1} = C_{02} \frac{d}{dt} [(V_{n,m-1} - V_{n,m}) - \delta_2 (V_{n,m-1} - V_{n,m})^2]$, and $\frac{dQ_{n,m}}{dt} = I_{n-1,m}^1 - I_{n,m}^1 + I_{n,m-1}^2 - I_{n,m}^2$. It therefore follows that the differential equations governing the dynamics of signals in the network are

$$\begin{aligned} \frac{d^2 V_{n,m}}{dt^2} - \alpha \frac{d^2 V_{n,m}^2}{dt^2} &= u_{01}^2 (V_{n+1,m} + V_{n-1,m} - 2V_{n,m}) + u_{02}^2 (V_{n,m+1} + V_{n,m-1} - 2V_{n,m}) + C_{r1} \frac{d^2}{dt^2} (V_{n-1,m} + V_{n+1,m} - 2V_{n,m}) \\ &+ C_{r2} \frac{d^2}{dt^2} (V_{n,m-1} + V_{n,m+1} - 2V_{n,m}) - \eta_1 \frac{d^2}{dt^2} [(V_{n-1,m} - V_{n,m})^2 - (V_{n,m} - V_{n+1,m})^2] \\ &- \eta_2 \frac{d^2}{dt^2} [(V_{n,m-1} - V_{n,m})^2 - (V_{n,m} - V_{n,m+1})^2], \end{aligned} \quad (1)$$

with $n = 1, 2, \dots, N$; $m = 1, 2, \dots, M$; $u_{01}^2 = 1/L_1 C_0$; $u_{02}^2 = 1/L_2 C_0$; $C_{r1} = C_{01}/C_0$; $C_{r2} = C_{02}/C_0$; $\eta_1 = \delta_1 C_{r1}$; and $\eta_2 = \delta_2 C_{r2}$. Here N and M correspond to the number of cells considered in the n and m directions, respectively. Equation (1) has been used to describe the dynamics of transverse solitary waves in the specific case where the capacitor C_i in the series branch is linear, that is, for $\delta_i = 0$ with $i = 1, 2$ [11]. In this study, the following characteristic network parameters will be considered [1,4,11]:

$$\begin{aligned} V_b &= 2 \text{ V}, \quad C_0 = 320 \text{ pF}, \quad \alpha = 0.21 \text{ V}^{-1}, \\ C_{01} &= C_{02} = 96 \text{ pF}, \quad L_1 = L_2 = 0.47 \text{ mH}, \\ \delta_1 &= \delta_2 = 0.21 \text{ V}^{-1}. \end{aligned} \quad (2)$$

As in previous work [11], we use the continuum limit approximation. This continuity assumption is valid only if the excited wavelengths are much longer than the cell sizes and the perturbation voltage represented by V is sufficiently small compared with its value in the equilibrium state. We suppose that the

spacing between two adjacent sections in the n direction is h_1 and h_2 in the m direction. Letting $V_{n,m}(t) \rightarrow V(n', m', t)$ with $n' = nh_1$ and $m' = mh_2$, we obtain from Eq. (1) the following two-dimensional partial differential equation for the perturbed voltage V :

$$\begin{aligned} \frac{\partial^2}{\partial t^2} (V - \alpha V^2) - u_{01}^2 h_1^2 \frac{\partial^2 V}{\partial n'^2} - u_{02}^2 h_2^2 \frac{\partial^2 V}{\partial m'^2} \\ - C_{r1} h_1^2 \frac{\partial^2}{\partial t^2} \left(\frac{\partial^2 V}{\partial n'^2} \right) - 2\eta_1 h_1^3 \frac{\partial^2}{\partial t^2} \left(\frac{\partial^2 V}{\partial n'^2} \frac{\partial V}{\partial n'} \right) \\ - C_{r2} h_2^2 \frac{\partial^2}{\partial t^2} \left(\frac{\partial^2 V}{\partial m'^2} \right) - 2\eta_2 h_2^3 \frac{\partial^2}{\partial t^2} \left(\frac{\partial^2 V}{\partial m'^2} \frac{\partial V}{\partial m'} \right) = 0. \end{aligned} \quad (3)$$

Introducing new variables $x = n'/h_1$ and $y = m'/h_2$, Eq. (3) becomes

$$\begin{aligned} \frac{\partial^2}{\partial t^2} (V - \alpha V^2) - u_{01}^2 \frac{\partial^2 V}{\partial x^2} - u_{02}^2 \frac{\partial^2 V}{\partial y^2} \\ - C_{r1} \frac{\partial^2}{\partial t^2} \left(\frac{\partial^2 V}{\partial x^2} \right) - 2\eta_1 \frac{\partial^2}{\partial t^2} \left(\frac{\partial^2 V}{\partial x^2} \frac{\partial V}{\partial x} \right) \\ - C_{r2} \frac{\partial^2}{\partial t^2} \left(\frac{\partial^2 V}{\partial y^2} \right) - 2\eta_2 \frac{\partial^2}{\partial t^2} \left(\frac{\partial^2 V}{\partial y^2} \frac{\partial V}{\partial y} \right) = 0. \end{aligned} \quad (4)$$

Equation (4) is the equation governing the propagation of the wave in the nonlinear electrical transmission line. To find its traveling-wave solution, we introduce the wave variable [13]

$$V(x, y, t) = V(z), \quad z = k_1 x + k_2 y - v_0 t, \quad (5)$$

where v_0 is the speed of the traveling wave and k_i with $i = 1, 2$ are arbitrary real constants. Accordingly, after two successive integrations, Eq. (4) leads to the ordinary differential equation (ODE)

$$\frac{d^2 V}{dz^2} + c \frac{d^2 V}{dz^2} \frac{dV}{dz} - aV + bV^2 = 0, \quad (6)$$

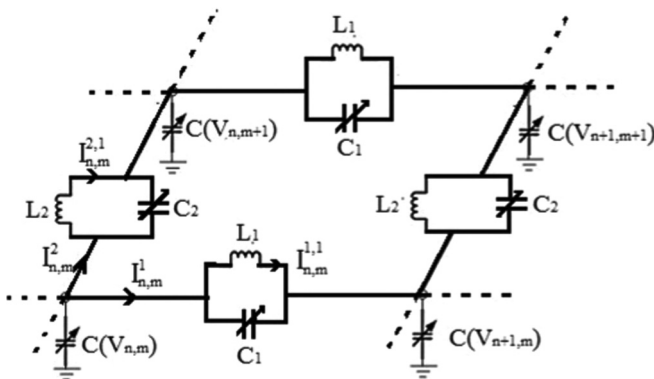


FIG. 1. Schematic representation of a part of the bidimensional transmission line with quadratic nonlinear dispersion. Each cell contains the nonlinear capacitor $C(V)$ in the shunt branch which induces the standard nonlinearity, while in the series propagation and transverse branches, we have the linear inductors L_1 and L_2 and the nonlinear capacitors C_1 and C_2 .

this by assuming that the integration constants are equal to zero. The expressions of the various coefficients of (6) are

$$a = \frac{v_0^2 - \bar{u}_{01}^2 - \bar{u}_{02}^2}{v_0^2(\bar{C}_{r1} + \bar{C}_{r2})}, \quad b = \frac{\alpha}{\bar{C}_{r1} + \bar{C}_{r2}}, \quad c = \frac{2(\bar{\eta}_1 k_1 + \bar{\eta}_2 k_2)}{\bar{C}_{r1} + \bar{C}_{r2}}, \quad (7)$$

with $\bar{u}_{01}^2 = u_{01}^2 k_1^2$, $\bar{u}_{02}^2 = u_{02}^2 k_2^2$, $\bar{C}_{r1} = C_{r1} k_1^2$, $\bar{C}_{r2} = C_{r2} k_2^2$, $\bar{\eta}_1 = \eta_1 k_1^2$, and $\bar{\eta}_2 = \eta_2 k_2^2$. Traveling-wave solutions such as (6) strongly depend on the sign of the coefficients a , b , and c . From their expressions (7), the following remarks can be made.

(i) The sign and the value of the linear coefficient a depends on the magnitude of the traveling-wave speed v_0 . It is negative, absent, and positive, respectively, if $v_0^2 < u_0^2$, $v_0^2 = u_0^2$, and $v_0^2 > u_0^2$, with $u_0^2 = \bar{u}_{01}^2 + \bar{u}_{02}^2$.

(ii) The coefficient b is always positive and is induced by the classic nonlinearity of the capacitor C in the shunt branch of Fig. 1.

(iii) The presence of the nonlinear dispersion term proportional to c in the ODE (6) is the contribution of the nonlinear component considered in the capacitance-voltage relationship in the series branch. Its sign still depends on the free parameters k_i with $i = 1, 2$. Thus, according to the magnitude and sign of this parameters, c can take any value and any sign. Recently, a bifurcation of the solutions of Eq. (6) has been investigated in the specific case where $c = 0$, which corresponds to $\delta_i = 0$ with $i = 1, 2$. Taking the nonlinearity of any of the capacitors in the series branches into account fundamentally modifies the governing equation. Thus, it becomes important to study the effect of this quadratic dispersion on the behavior of the traveling-wave solutions of Eq. (6).

III. PHASE PLANE ANALYSIS

Equation (6) can be reduced to a two-dimensional dynamical system

$$\frac{dV}{dz} = W, \quad \frac{dW}{dz} = \frac{V(a - bV)}{1 + cW}. \quad (8)$$

We note that if $c \neq 0$, Eq. (8) is a singular traveling-wave system. It has a singular straight line defined by $W = -1/c$. To avoid this line temporarily, we consider the transformation $dz = (1 + cW)d\xi$ under which the system (8) becomes

$$\frac{dV}{d\xi} = W(1 + cW), \quad \frac{dW}{d\xi} = V(a - bV). \quad (9)$$

These two systems have the same Hamiltonian defined as

$$H(V, W) = \frac{1}{2}(W^2 - aV^2) + \frac{1}{3}(cW^3 + bV^3) = h, \quad (10)$$

where h is a constant. This Hamiltonian can be obtained by integrating Eq. (6) after multiplying it by $\frac{dV}{dz}$ and then setting $\frac{dV}{dz} = W$ in the result.

We observe that the system (9) has many fixed points or stationary states depending on the value of its three coefficients a , b , and c . We notice first that $A_0(0, 0)$ is always an equilibrium point of Eq. (9) independently of the parameters' values. If $c = 0$, that is, for the linear capacitor C_1 and C_2 , Eq. (9) has one additional equilibrium point [11]. When $c \neq 0$, two relevant cases can be distinguished: For $a = 0$, Eq. (9) has

one additional equilibrium point $A_1(0, -1/c)$, while for $a \neq 0$, Eq. (9) has three additional equilibrium points $A_1(0, -1/c)$, $A_2(a/b, 0)$, and $A_3(a/b, -1/c)$.

Let $M(V_j, W_j)$ be the coefficient matrix of the linearized system (7) at an equilibrium point (V_j, W_j) and $J(V_j, W_j)$, the associated Jacobian determinant. Also denote by $\text{Tr}(M(\psi_j, W_j))$ the trace of the matrix $M(\psi_j, W_j)$. Thus, we have

$$\begin{aligned} J_0 &= J(0, 0) = -a, & J_1 &= J(0, -1/c) = a, \\ J_2 &= J(a/b, 0) = a, & J_3 &= J(a/b, -1/c) = -a. \end{aligned} \quad (11)$$

By the theory of planar dynamical systems [14–16], we know that for an equilibrium point of a planar integrable system, if $J < 0$, then the equilibrium point is a saddle point; if $J > 0$ and $\text{Tr}(M(\psi_j, W_j)) = 0$, then it is a center point; if $J > 0$ and $[\text{Tr}(M(\psi_j, W_j))]^2 - 4J(\psi_j, W_j) \geq 0$, then it is a node point; if $J = 0$ and the Poincaré index of the equilibrium point is 0, then this equilibrium point is a cusp.

Hereafter, we use the definitions

$$\begin{aligned} h_0 &= H(0, 0) = 0, & h_1 &= H(0, -1/c) = 1/6c^2, \\ h_2 &= H(a/b, 0) = -a^3/6b^2, \\ h_3 &= H(a/b, -1/c) = (b^2 - a^3c^2)/6b^2c^2, \end{aligned} \quad (12)$$

in which $H(V, W)$ designates the first integral defined in Eq. (10). We then note that for given values of the system's parameters $h_3 = h_0 = 0$ and $h_1 = h_2$, respectively, if the front velocity v_0 takes the critical values v_{0c-} and v_{0c+} . In fact, based on Eq. (12), these conditions are satisfied if $a = (b/c)^{2/3}$ and $a = -(b/c)^{2/3}$, respectively. Thus, using the expressions of a , b , and c given by Eq. (7), we obtain

$$v_{0c\pm}^2 = \frac{u_0^2}{1 \pm C_r(\alpha/2\eta)^{2/3}}, \quad (13)$$

with $\eta = \bar{\eta}_1 k_1 + \bar{\eta}_2 k_2$ and $C_r = \bar{C}_{r1} + \bar{C}_{r2}$. By using the above information, we can easily do a qualitative analysis of the systems (8) and (9). It is really important to specify that the phase orbits defined by the system (9) will determine all traveling-wave solutions of Eq. (6). In particular, each trajectory of the phase portraits of the system (8) represents a solution of Eq. (6). Hence, with a view to clearly see the effect of the quadratic nonlinear dispersion, which was not considered in [11], on the bifurcation of these solutions, we take in this work $\delta_i \neq 0$ ($i = 1, 2$). According to the value of the traveling-wave speed, different phase portraits of the system (9) are presented in Figs. 2 and 3.

For the phase portrait given by Fig. 2, $v_0 = u_0$ and $k_1 = k_2 = 1$. In this case, we have $a = 0$ and the system (9) has two equilibrium points, namely, $A_0(0, 0)$ and $A_1(0, -1/c)$, which are the cusps.

For the phase portrait given by Fig. 3, $v_0 \neq u_0$ and $k_1 = k_2 = 1$. In this case, we have $a \neq 0$ and the system (9) has four equilibrium points at $A_0(0, 0)$, $A_1(0, -1/c)$, $A_2(a/b, 0)$, and $A_3(a/b, -1/c)$. For $v_0 < u_0$, that is, $a < 0$, A_0 and A_3 are centers and A_1 and A_2 are saddle points. On the other hand, if $v_0 > u_0$, that is, $a > 0$, A_0 and A_3 become saddle points while A_1 and A_2 are centers.

From the above qualitative results, some conclusions can be made. First, the velocity v_0 plays a major role in

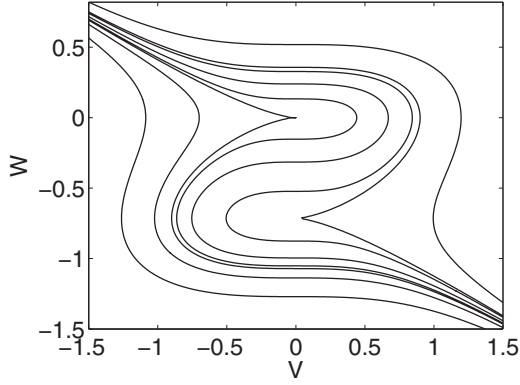


FIG. 2. Bifurcations of phase portraits of the system (9) in the (V, W) phase plane with the parameters (2) and $v_0 = u_0$ and $k_1 = k_2 = 1$.

the determination of the type of traveling waves propagating in our network. Next, the system (9) admits several kinds of traveling-wave solutions, namely, periodic waves, solitary waves, and breaking waves, which correspond to homoclinic orbits, periodic orbits, and heteroclinic orbits or arch curves of the phase portraits, respectively. Finally, the number of equilibrium points of the system (9) and their nature are independent of the sign of the coefficient c .

Note that, with fixed values of the network parameters, the signs of k_i , with $i = 1, 2$, do not play a crucial role in obtaining qualitatively different phase portraits of the system. In other words, we could vary k_i with fixed values of network parameters, but this does not give us any significantly different qualitative results. In fact, reversing the sign of k_i ($k_i < 0$), the

sign of the coefficient c in Eq. (6) also changes ($c < 0$). In this case, the different corresponding phase portraits are deduced from Figs. 2 and 3 through a simple symmetry about the horizontal axis, that is, $V = 0$. Hence, the dynamical behavior of the system is not affected by the sign of k_i . In addition, by reversing the sign of both k_i and z , the system remains invariant.

IV. SOLITARY PROFILE SOLUTIONS OF EQ. (6)

In this section we focus our attention on the computation of the exact parametric representations of the traveling-wave solutions of the characteristic ordinary differential equation of the system which is modeled by Eq. (1). We restrict ourselves, for simplicity, to the solitary-wave solutions which correspond to homoclinic orbits or heteroclinic orbits of the system (8). These are defined by $H(V, W) = h_j$, where h_j (with $j = 0, 1, 2, 3$) are given by Eq. (12). Notice that the points $A_1(0, -1/c)$ and $A_3(a/b, -1/c)$ are not the equilibrium points of the system (8). We begin by introducing the variables

$$V = \bar{V} + V_j, \quad W = \bar{W} + W_j, \quad (14)$$

with V_j and W_j the coordinates of equilibrium point A_j . For example, if $j = 0$, we have $V_0 = 0$ and $W_0 = 0$, which are the coordinates of equilibrium A_0 . In this specific case, $V = \bar{V}$ and $W = \bar{W}$. Using Eq. (14), the system (9) becomes

$$\frac{d\bar{V}}{d\xi} = \bar{W}(\epsilon'_j + c\bar{W}), \quad \frac{d\bar{W}}{d\xi} = \bar{V}(a\epsilon_j - b\bar{V}) \quad (15)$$

and has the Hamiltonian

$$H(\bar{V}, \bar{W}) - h_j = \frac{1}{2}(\epsilon'_j \bar{W}^2 - a\epsilon_j \bar{V}^2) + \frac{1}{3}(c\bar{W}^3 + b\bar{V}^3) = 0, \quad (16)$$

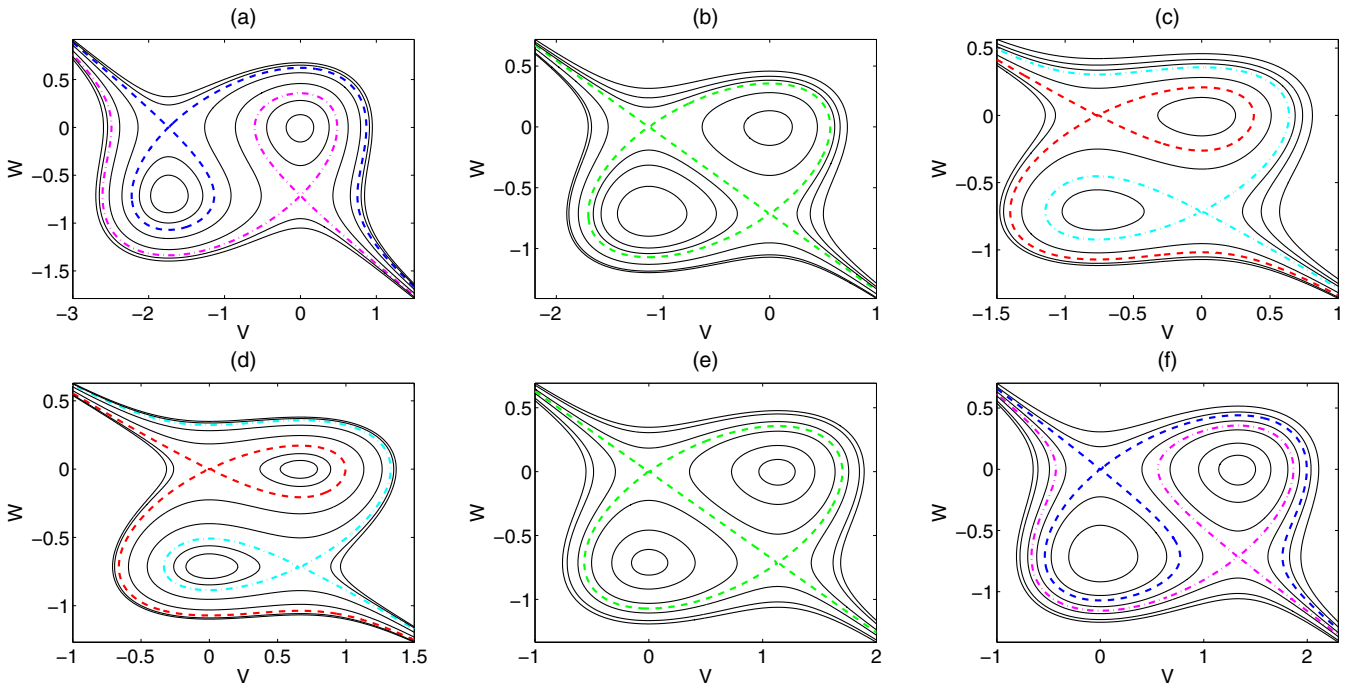


FIG. 3. Bifurcations of phase portraits of the system (9) in the (V, W) phase plane with the parameters (2) and $k_1 = k_2 = 1$: (a) $0 < v_0 < v_{0c+}$, (b) $v_0 = v_{0c+}$, (c) $v_{0c+} < v_0 < u_0$, (d) $u_0 < v_0 < v_{0c-}$, (e) $v_0 = v_{0c-}$, and (f) $v_0 > v_{0c-}$.

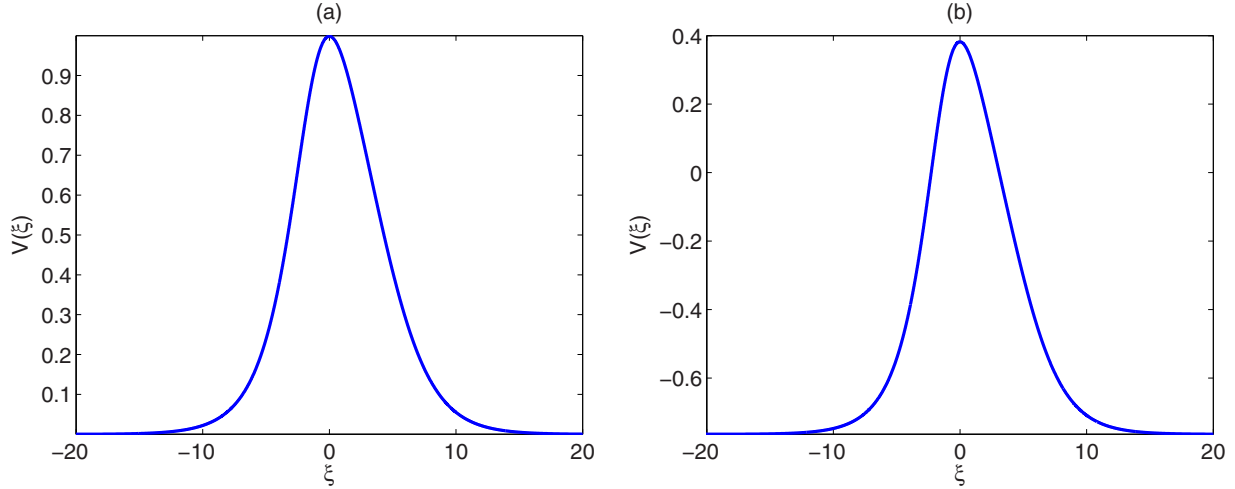


FIG. 4. Shape of the single solitary waves of (6) with the parameters (2) and $k_1 = k_2 = 1$: (a) bright soliton (25) for $v_0 = 3.934 \times 10^6$ rad/s and (b) gray soliton (28) for $v_0 = 3.387 \times 10^6$ rad/s.

with $j = 0, 1, 2, 3$. Here ϵ'_j and ϵ_j can be either +1 or -1 depending on the equilibrium point. For instance, at point A_0 , $\epsilon'_0 = \epsilon_0 = 1$; at point A_1 , $\epsilon'_1 = -\epsilon_1 = -1$; at point A_2 , $\epsilon'_2 = -\epsilon_2 = 1$; and at point A_3 , $\epsilon'_3 = \epsilon_3 = -1$. Now, to investigate the solitary-wave solutions of this system, we use the polar coordinates

$$\bar{V} = \rho \cos(\theta), \quad \bar{W} = \rho \sin(\theta) \quad (17)$$

and system (15) and the first integral (16) become, respectively,

$$\begin{aligned} \frac{d\rho}{d\xi} &= \rho^2 \cos(\theta) \sin(\theta) (c \sin(\theta) - b \cos(\theta)) \\ &\quad + \rho \cos(\theta) \sin(\theta) (a\epsilon_j + \epsilon'_j), \end{aligned} \quad (18a)$$

$$\begin{aligned} \frac{d\theta}{d\xi} &= -\rho (b \cos^3(\theta) + c \sin^3(\theta)) \\ &\quad + a\epsilon_j \cos^2(\theta) - \epsilon'_j \sin^2(\theta), \end{aligned} \quad (18b)$$

and

$$\begin{aligned} H(\rho, \theta) - h_j &= \frac{1}{2} \rho^2 (\epsilon'_j \sin^2(\theta) - a\epsilon_j \cos^2(\theta)) \\ &\quad + \frac{1}{3} \rho^3 (c \sin^3(\theta) + b \cos^3(\theta)) = 0. \end{aligned} \quad (19)$$

From the Hamiltonian values defined by (19) it follows that

$$\rho(\theta) = \frac{3 a \epsilon_j \cos^2(\theta) - \epsilon'_j \sin^2(\theta)}{2 (c \sin^3(\theta) + b \cos^3(\theta))}. \quad (20)$$

Setting $\mu(\xi) = \tan[\theta(\xi)]$, Eq. (20) can be put in the form

$$\rho(\xi) = \frac{3}{2} \frac{a\epsilon_j - \epsilon'_j \mu(\xi)^2}{\cos(\theta) (b + c\mu(\xi)^3)}. \quad (21)$$

According to Eq. (17), we find the following parametric representation for the solutions $\bar{V}(\xi)$ and $\bar{W}(\xi)$ of the system (9):

$$\bar{V}(\xi) = \frac{3}{2} \frac{a\epsilon_j - \epsilon'_j \mu(\xi)^2}{b + c\mu(\xi)^3}, \quad (22)$$

$$\bar{W}(\xi) = \frac{3\mu(\xi)}{2} \frac{a\epsilon_j - \epsilon'_j \mu(\xi)^2}{b + c\mu(\xi)^3}. \quad (23)$$

From (18b) we have

$$\xi = -2 \int_{\theta_0}^{\theta} \frac{1 + \tan^2(\theta)}{a\epsilon_j - \epsilon'_j \tan^2(\theta)} d\theta = \int_{\mu_0}^{\mu} \frac{-2}{a\epsilon_j - \epsilon'_j \mu^2} d\mu. \quad (24)$$

The exact solutions of Eq. (8) given by Eqs. (22) and (23) are definitively obtained from the results of the integral in Eq. (24). These kinds of results depend on both the relative magnitudes of the system's parameters and the value of the velocity v_0 as discussed below.

A. Bright and gray solitary waves of Eq. (8): $v_{0c+} < v_0 < u_0$ and $u_0 < v_0 < v_{0c-}$

When the speed of the traveling wave v_0 belongs to $]u_0, v_{0c-}[$ and $]v_{0c+}, u_0-]$, the phase portrait of the dynamical system (9) possesses some homoclinic orbits [Figs. 3(c) and 3(d)].

(i) Corresponding to the orbit of the system (9) that is homoclinic to A_0 , defined by $H(V, W) = h_0 = 0$ and enclosing the equilibrium point A_2 [red dashed curve in Fig. 3(d)], there exists a bright solitary-wave solution of the system (8). By using (24), one has $\mu(\xi) = \sqrt{a} \tanh(-\frac{\sqrt{a}}{2}\xi)$. Hence, Eqs. (22) and (23) lead to, respectively,

$$V(\xi) = \frac{3a}{2} \frac{1 - \tanh^2(-\frac{\sqrt{a}}{2}\xi)}{b + a^{3/2}c \tanh^3(-\frac{\sqrt{a}}{2}\xi)} \quad (25)$$

and

$$W(\xi) = \frac{3a^{3/2} \tanh(-\frac{\sqrt{a}}{2}\xi)}{2} \frac{1 - \tanh^2(-\frac{\sqrt{a}}{2}\xi)}{b + a^{3/2}c \tanh^3(-\frac{\sqrt{a}}{2}\xi)}. \quad (26)$$

Since $dz = (1 + cW)d\xi$, we have

$$z(\xi) = \xi + c \int_0^{\xi} W(\xi) d\xi, \quad (27)$$

with $W(\xi)$ given by Eq. (26). Equations (25) and (27) constitute the parametric representations of the solutions of the characteristic ODE (6) of the system.

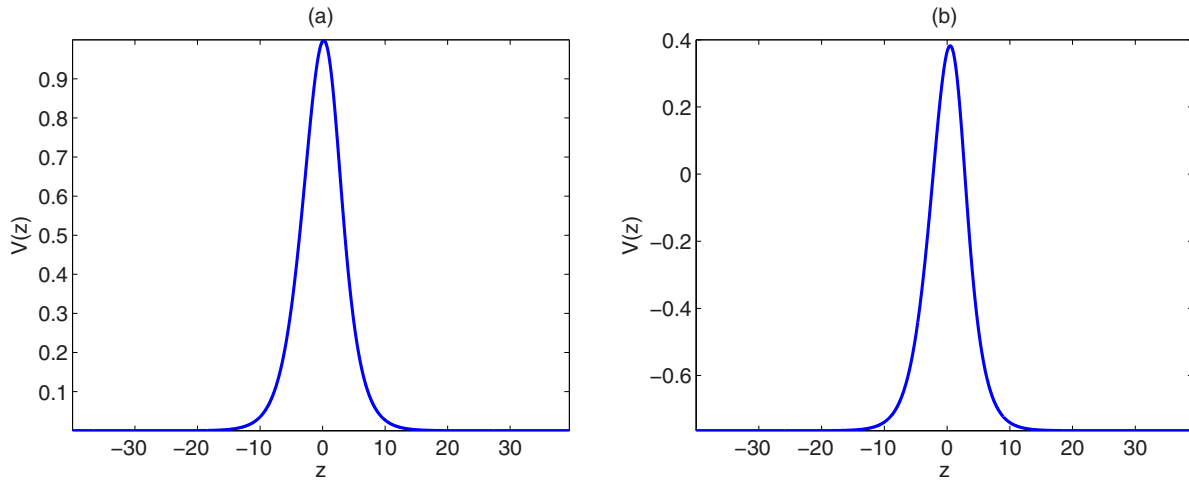


FIG. 5. Typical graph of the single bright and gray solitary waves of (6) in terms of the wave variable z , with the same parameters as in Fig. 4. The initial values for the triplet (V, W, z) are (a) $(4 \times 10^{-8}, 0, -40)$ and (b) $(a/b, 5 \times 10^{-9}, -40)$, with a and b computed from the parameters using Eq. (7).

(ii) Corresponding to the orbit of the system (9) defined by $H(V, W) = h_2$, which is homoclinic to A_2 and encloses the equilibrium point A_0 [red dashed curve in Fig. 3(c)], there exists a gray solitary-wave solution of the system (8). In this case, it follows from Eq. (24) that $\mu(\xi) = \sqrt{-a} \tanh(-\frac{\sqrt{-a}}{2}\xi)$. Thus, from (22) and (23) we obtain the parametric representation of the gray solitary-wave solution of Eq. (6) as

$$V(\xi) = -\frac{3a}{2} \frac{1 - \tanh^2(-\frac{\sqrt{-a}}{2}\xi)}{b + \sqrt{-a^3}c \tanh^3(-\frac{\sqrt{-a}}{2}\xi)} + \frac{a}{b}, \quad (28)$$

$$z(\xi) = \xi + c \int_0^\xi W(\xi) d\xi, \quad (29)$$

with

$$W(\xi) = -\frac{3\sqrt{-a^3} \tanh(-\frac{\sqrt{-a}}{2}\xi) [1 - \tanh^2(-\frac{\sqrt{-a}}{2}\xi)]}{2b + 2\sqrt{-a^3}c \tanh^3(-\frac{\sqrt{-a}}{2}\xi)}.$$

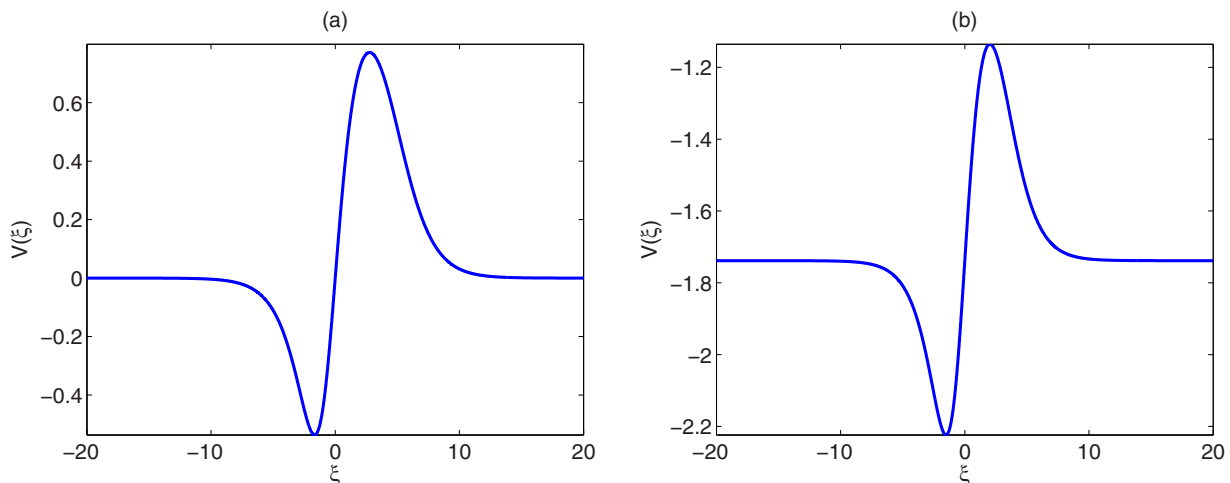


FIG. 6. The N-shape solitary wave of (6) with the parameters (2) and $k_1 = k_2 = 1$: (a) Eq. (30) for $v_0 = 4.298 \times 10^6$ rad/s and (b) Eq. (32) for $v_0 = 3.123 \times 10^6$ rad/s.

The graphical representations of these solutions (25) and (28) are shown in Fig. 4 with the network parameters (2) and for a suitable value of the wave velocity v_0 .

Note that Eqs. (27) and (29) exhibit a complex dependence on the expression $W(\xi)$. This complexity prevents the determination of the explicit analytical expression of the solutions of Eq. (6) in terms of the wave variable z . Nevertheless, typical graphs of these solutions can be obtained numerically by integrating the system consisting of Eq. (9) and $dz/d\xi = (1 + cW)$. For instance, the graphical representations of bright (25) and gray (28) solitary waves in terms of the wave variable z are shown in Fig. 5 with the same parameters as in Fig. 4.

B. N-shape wave profile consisting of three breaking waves of Eq. (8): $0 < v_0 < v_{0c+}$ and $v_0 > v_{0c-}$

For small as well as high values of the wave speed, that is, v_0 belonging to $]0, v_{0c+}[$ and $v_0 > v_{0c-}$, there exist homoclinic orbits of the dynamical system (9) [Figs. 3(a) and 3(f)].

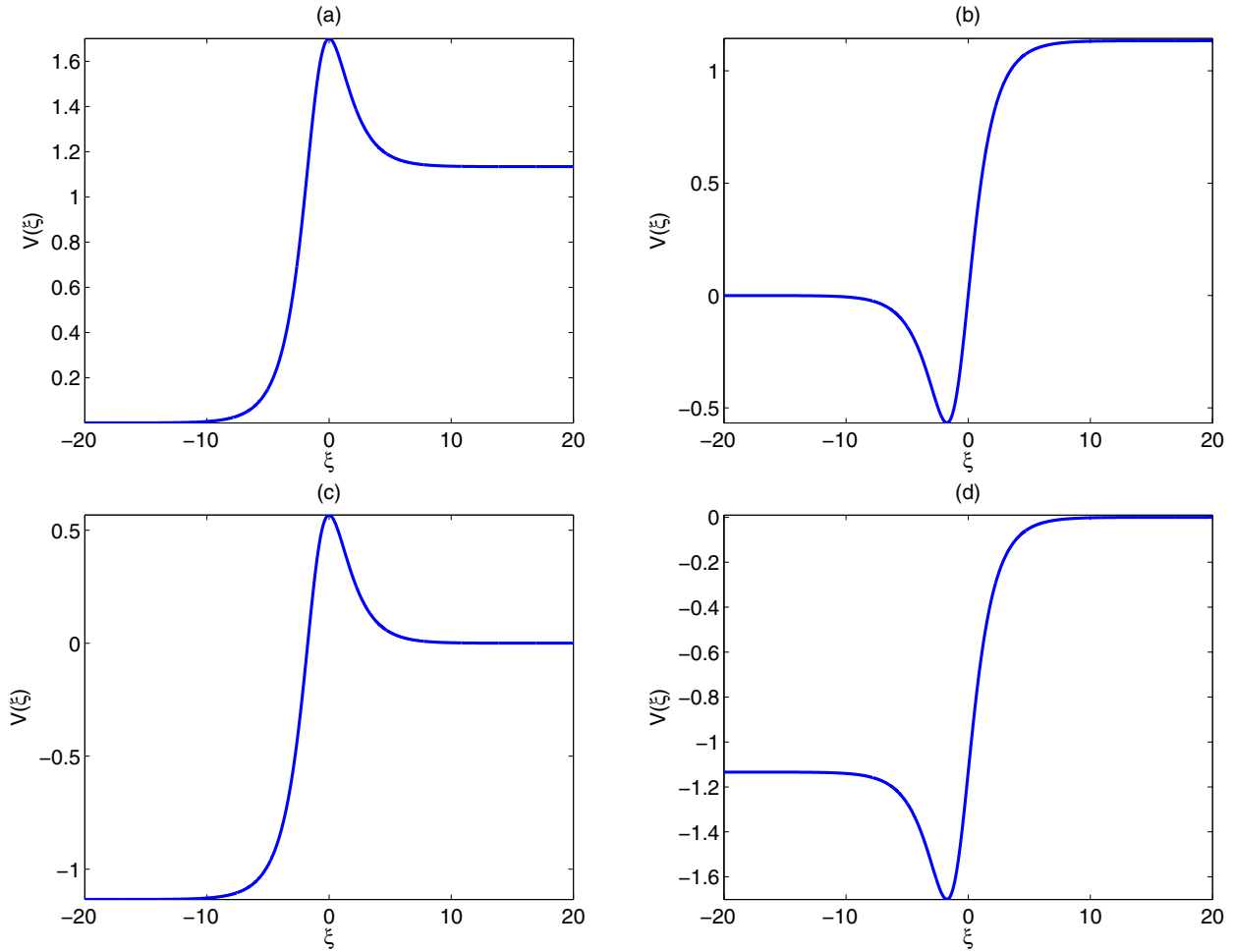


FIG. 7. Shape wave profile of (6) with the parameters (2) and $k_1 = k_2 = 1$: (a) Eq. (34) for $\nu_0 = 4.180 \times 10^6$ rad/s, (b) Eq. (36) for $\nu_0 = 4.180 \times 10^6$ rad/s, (c) Eq. (38) for $\nu_0 = 3.279 \times 10^6$ rad/s, and (d) Eq. (40) for $\nu_0 = 3.279 \times 10^6$ rad/s.

(i) Corresponding to the homoclinic orbit of the system (9) at A_0 , defined by $H(V, W) = h_0 = 0$ and enclosing the equilibrium point A_1 [blue dashed curve in Fig. 3(f)], there exist three breaking-wave solutions of the system (8). Based on Eq. (24), the function $\mu(\xi)$ can be written as $\mu(\xi) = \sqrt{a} \coth(\frac{-\sqrt{a}}{2}\xi)$. Hence, we obtain from (22) and (23) that

$$V(\xi) = \frac{3a}{2} \frac{1 - \coth^2(\frac{-\sqrt{a}}{2}\xi)}{b + a^{3/2}c \coth^3(\frac{-\sqrt{a}}{2}\xi)}, \quad (30)$$

$$z(\xi) = \xi + c \int_0^\xi W(\xi) d\xi, \quad (31)$$

where

$$W(\xi) = \frac{3a^{3/2} \coth(\frac{-\sqrt{a}}{2}\xi)}{2} \frac{1 - \coth^2(\frac{-\sqrt{a}}{2}\xi)}{b + a^{3/2}c \coth^3(\frac{-\sqrt{a}}{2}\xi)}.$$

(ii) Corresponding to the homoclinic orbit of the system (9) at A_2 , defined by $H(V, W) = h_2$ and enclosing the equilibrium point A_3 [blue dashed curve in Fig. 3(a)], there exist three breaking-wave solutions of the system (8). Based on Eq. (24), the function $\mu(\xi)$ can be written as

$\mu(\xi) = \sqrt{-a} \coth(\frac{-\sqrt{-a}}{2}\xi)$. Hence, we obtain from (22) and (23) that

$$V(\xi) = \frac{3a}{2} \frac{-1 + \coth^2(\frac{-\sqrt{-a}}{2}\xi)}{b + (-a)^{3/2}c \coth^3(\frac{-\sqrt{-a}}{2}\xi)} + \frac{a}{b}, \quad (32)$$

$$z(\xi) = \xi + c \int_0^\xi W(\xi) d\xi, \quad (33)$$

where

$$W(\xi) = \frac{3(-a)^{3/2} \coth(\frac{-\sqrt{-a}}{2}\xi) [-1 + \coth^2(\frac{-\sqrt{-a}}{2}\xi)]}{2b + 2c(-a)^{3/2} \coth^3(\frac{-\sqrt{-a}}{2}\xi)}.$$

The graphical representations of the different profiles of breaking waves defined by Eqs. (30) and (32) are shown in Fig. 6 with the network parameters (2).

C. Other shape wave profiles of Eq. (8): $\nu_0 = \nu_{0c+}$ and $\nu_0 = \nu_{0c-}$

(i) Corresponding to the two heteroclinic orbits of (9) [green dashed curves in Fig. 3(e)] connecting the equilibrium points A_0 and A_3 and defined by $H(V, W) = h_0 = h_3 = 0$,

there are breaking-wave solutions of the system (8). Based on Eq. (24), the function $\mu(\xi)$ can be written as $\mu(\xi) = \sqrt{a} \tanh(\frac{-\sqrt{a}}{2}\xi)$ and $\mu(\xi) = \sqrt{a} \coth(\frac{-\sqrt{a}}{2}\xi)$ for the lower and upper heteroclinic orbits, respectively. By using Eqs. (22) and (23), respectively, complete calculations yield

$$V(\xi) = \frac{3a}{2b} \frac{1 - \tanh^2(-\frac{\sqrt{a}}{2}\xi)}{1 + \tanh^3(-\frac{\sqrt{a}}{2}\xi)}, \quad (34)$$

$$z(\xi) = \xi + c \int_0^\xi W(\xi) d\xi, \quad (35)$$

with

$$W(\xi) = \frac{3a^{3/2} \tanh(-\frac{\sqrt{a}}{2}\xi)}{2b} \frac{1 - \tanh^2(-\frac{\sqrt{a}}{2}\xi)}{1 + \tanh^3(-\frac{\sqrt{a}}{2}\xi)},$$

for the bottom heteroclinic orbit and

$$V(\xi) = \frac{3a}{2b} \frac{1 - \coth^2(-\frac{\sqrt{a}}{2}\xi)}{1 + \coth^3(-\frac{\sqrt{a}}{2}\xi)} \quad (36)$$

$$z(\xi) = \xi + c \int_0^\xi W(\xi) d\xi, \quad (37)$$

where

$$W(\xi) = \frac{3a^{3/2} \coth(-\frac{\sqrt{a}}{2}\xi)}{2b} \frac{1 - \coth^2(-\frac{\sqrt{a}}{2}\xi)}{1 + \coth^3(-\frac{\sqrt{a}}{2}\xi)},$$

for the top heteroclinic orbit.

(ii) Corresponding to the two heteroclinic orbits of (9) [green dashed curves in Fig. 3(b)] connecting the equilibrium points A_1 and A_2 [Fig. 3(b)] and defined by $H(V, W) = h_1 = h_2 = 0$, there are breaking-wave solutions of the system (8). Based on Eq. (24), the function $\mu(\xi)$ can be written as $\mu(\xi) = \sqrt{-a} \tanh(\frac{-\sqrt{-a}}{2}\xi)$ and $\mu(\xi) = \sqrt{-a} \coth(\frac{-\sqrt{-a}}{2}\xi)$ for the bottom and top heteroclinic orbits, respectively. By using Eqs. (22) and (23), respectively, complete calculations yield

$$V(\xi) = -\frac{3a}{2b} \frac{1 - \tanh^2(-\frac{\sqrt{-a}}{2}\xi)}{1 + \tanh^3(-\frac{\sqrt{-a}}{2}\xi)} + \frac{a}{b}, \quad (38)$$

$$z(\xi) = \xi + c \int_0^\xi W(\xi) d\xi, \quad (39)$$

with

$$W(\xi) = -\frac{3\sqrt{-a^3} \tanh(-\frac{\sqrt{-a}}{2}\xi)[1 - \tanh^2(-\frac{\sqrt{-a}}{2}\xi)]}{2b[1 + \tanh^3(-\frac{\sqrt{-a}}{2}\xi)]},$$

for bottom heteroclinic orbit and

$$V(\xi) = \frac{3a}{2b} \frac{-1 + \coth^2(-\frac{\sqrt{-a}}{2}\xi)}{1 + \coth^3(-\frac{\sqrt{-a}}{2}\xi)} + \frac{a}{b}, \quad (40)$$

$$z(\xi) = \xi + c \int_0^\xi W(\xi) d\xi, \quad (41)$$

where

$$W(\xi) = \frac{3(-a)^{3/2} \coth(-\frac{\sqrt{-a}}{2}\xi)[-1 + \coth^2(-\frac{\sqrt{-a}}{2}\xi)]}{2b[1 + \coth^3(-\frac{\sqrt{-a}}{2}\xi)]},$$

for top heteroclinic orbit. The different profiles of these breaking waves defined by Eqs. (34), (36), (38), and (40) are shown in Fig. 7 with the network parameters (2).

V. CONCLUSION

We have investigated the qualitative structures of traveling waves in a bidimensional model of an inductor-capacitor network with nonlinear dispersion. This model is different from the models discussed in the literature by considering the contribution of the quadratic nonlinear limit in the capacitance-voltage relationship in the series branch. For amplitude signals lower than the dc bias voltage and using the continuum limit approximation, we reduced the differential equations governing the propagation of the signal voltage in the network to a $(2+1)$ -dimensional partial differential equation. Through a simple change of variables, we transformed the latter to an ODE. The existence of traveling-wave solutions including the solitary-wave profiles of the obtained equation has been proved by means of the bifurcation method of dynamical systems. We have remarked that the values of wave speed influence considerably the type of wave solution in the system. The exact parametric representations of these wave solutions corresponding to some particular orbits of the system were derived and their two-dimensional graphics were given.

From the interesting results obtained in this work, we see clearly that the nonlinear dispersion plays a significant role in the model of the coupled inductor-capacitor network and can be used to obtain various solitary-wave profile solutions. Among these profiles, only the bright and gray solitary type were obtained in [11] for physically realistic parameters of the network. Others profiles are solutions in the context of the coupled nonlinear transmission lines. The stability of these solutions and the integrability of Eq. (4) are important subjects that should be considered in future investigations.

-
- [1] M. Remoissenet, *Waves Called Solitons*, 3rd ed. (Springer, Berlin, 1999).
 [2] J. C. Comte and P. Marquié, *Chaos Soliton. Fractal.* **29**, 307 (2006).
 [3] F. B. Pelap, J. H. Kamga, S. B. Yamgoué, S. M. Ngounou, and J. E. Ndeco, *Phys. Rev. E* **91**, 022925 (2015).
 [4] E. Kengne and W. M. Liu, *Phys. Rev. E* **97**, 052205 (2018).

- [5] G. R. Deffo, S. B. Yamgoué, and F. B. Pelap, *Phys. Rev. E* **98**, 062201 (2018).
 [6] S. Abdoukary, A. Mohamadou, and T. Beda, *Commun Nonlinear Sci. Numer. Simul.* **16**, 3525 (2001).
 [7] S. D. Yamigno, *J. Mod. Phys.* **5**, 394 (2014).
 [8] E. Kengne, Abdourahman, and A. Lakhssassi, *Chin. J. Phys.* **54**, 352 (2016).

- [9] G. R. Deffo, S. B. Yamgoué, and F. B. Pelap, *Eur. Phys. J. B* **91**, 242 (2018).
- [10] S. Abdoukary, T. Beda, S. Y. Doka, F. II Ndzana, L. Kavitha, and A. Mohamadou, *J. Mod. Phys.* **3**, 438 (2012).
- [11] S. B. Yamgoué, G. R. Deffo, E. Tala-Tebue, and F. B. Pelap, *Chin. Phys. B* **27**, 096301 (2018).
- [12] P. Marquie, J. M. Bilbault, and M. Remoissenet, *Phys. Rev. E* **49**, 828 (1994).
- [13] E. Tala-Tebue, D. C. Tsobgni-Fozap, A. Kenfack-Jiotsa, and T. C. Kofané, *Eur. Phys. J. Plus* **129**, 136 (2014).
- [14] A. Saha and P. Chatterjee, *Eur. Phys. J. D* **69**, 203 (2015).
- [15] J. Li, F. Chen, and A. S. Tchakoutio-Nguetcho, *Int. J. Bifurcat. Chaos* **25**, 1550062 (2015).
- [16] A. S. Tchakoutio Nguetcho, G. M. Nkeumaleu, and J. M. Bilbault, *Phys. Rev. E* **96**, 022207 (2017).